Representation of Antarctic Katabatic Winds in a High-Resolution GCM and a Note on Their Climate Sensitivity

MICHIEL R. VAN DEN BROEKE

Norwegian Polar Institute, Oslo, Norway

RODERIK S. W. VAN DE WAL

Institute for Marine and Atmospheric Research, Utrecht University, Utrecht, the Netherlands

MARTIN WILD

Department of Geography, Swiss Federal Institute of Technology, Zurich, Switzerland

(Manuscript received 7 October 1996, in final form 25 April 1997)

ABSTRACT

A high-resolution GCM (ECHAM-3 T106, resolution 1.1° × 1.1°) is found to simulate many characteristic features of the Antarctic climate. The position and depth of the circumpolar storm belt, the semiannual cycle of the midlatitude westerlies, and the temperature and wind field over the higher parts of the ice sheet are well simulated. However, the strength of the westerlies is overestimated, the annual latitudinal shift of the storm belt is suppressed, and the wintertime temperature and wind speed in the coastal areas are underestimated. These errors are caused by the imperfect simulation of the position of the subtropical ridge, the prescribed sea ice characteristics, and the smoothened model topography in the coastal regions. Ice shelves in the model are erroneously treated as sea ice, which leads to a serious overestimation of the wintertime surface temperature in these areas. In spite of these deficiencies, the model results show much improvement over earlier simulations. In a climate run, the model was forced to a new equilibrium state under enhanced greenhouse conditions (IPCC scenario A, doubled CO_2), which enables us to cast a preliminary look at the climate sensitivity of Antarctic katabatic winds. Summertime katabatic winds show a decrease of up to 15% in the lower parts of the ice sheet, as a result of the destruction of the surface inversion by increased absorption of solar radiation (temperature–albedo feedback). On the other hand, wintertime near-surface winds increase by up to 10% owing to a deepening of the circumpolar trough. As a result, the model predicts that the annual mean wind speed remains within 10% of its present value in a doubled CO_2 climate, but with an increased amplitude of the annual cycle.

1. Introduction

The representation of the Antarctic climate in general circulation models (GCMs) has improved considerably during the last decade (Simmonds 1990), partly as a result of increased model resolution and partly because physical parameterizations have been improved. Tzeng et al. (1993) studied the performance of the National Center for Atmospheric Research (NCAR) CCM1 over Antarctica and found that, in spite of the coarse horizontal resolution of 4.5° lat × 7.5° long (about 500 × 500 km), this model was able to simulate several synoptic and mesoscale features of the Antarctic climate. CCM2, an updated version of the model with a resolution of 2.8° × 2.8°, gave very much improved results (Tzeng et al. 1994). Genthon and Braun (1995) found good agreement between observations and the climatology of the European Centre for Medium-Range Weather Forecasts (ECMWF) analyses, which are based on GCM-generated parameter fields that are corrected to observations every 6 h. However, the simulated surface climate did not appear to be superior to those obtained with GCMs in pure climate mode, that is, which are not constrained by observations (Connolley and Cattle 1994; Genthon 1994). The present developments are encouraging, and the use of GCMs will play an important role in future meteorological, climatological, and glaciological research of the polar regions (van den Broeke 1997).

Strong and persistent katabatic winds represent one of the most outstanding climatological features of Antarctica. These winds are forced by the continuous cooling of air overlying the sloping Antarctic ice sheet. Model studies suggest that the Antarctic katabatic wind circulation influences the strength of the polar vortex and

Corresponding author address: Dr. Michiel R. van den Broeke, Norwegian Polar Institute, P.O. Box 5072 Majorstua, N-0301 Oslo, Norway.
E-mail: michiel@npolar.no

FIG. 1. Map of Antarctica with positions of selected stations. Also shown are the 1500-, 2500-, and 3500-m elevation contours.

vice versa (Yasunari and Kodama 1993; Simmonds and Law 1995), and enhances the formation of mesocyclones in the coastal areas (Gallée 1995). They have a large impact on the local mass balance of the ice sheet, being responsible for the formation of blue ice areas (van den Broeke and Bintanja 1995a), while Loewe (1970) estimated that katabatic winds blow 6% of the annual accumulation on Antarctica into the sea. Several studies indicated a strong interaction exists between summertime katabatic winds and the overlying free atmosphere (e.g., Kodama et al. 1989; van den Broeke and Bintanja 1995b; Gallée et al. 1996). With the increased availability of data from manned and automatic weather stations (AWS), the data coverage over the continent has steadily improved during the last decades (Stearns et al. 1993; Allison et al. 1993). Observations of Antarctic katabatic winds are, therefore, quite numerous (e.g., Adélie Land, Wendler et al. 1993), which enables us to check the performance of GCMs over Antarctica.

In section 3 of this paper, we compare output of the ECHAM-3 GCM, run in T106 mode (resolution 1.1°, 160 by 320 grid points), with observations of the modern Antarctic near-surface climate. Ohmura et al. (1996) found that this model calculated the accumulation and temperature distribution over the Greenland and Antarctic ice sheets with unprecedented accuracy. Ohmura et al. (1994) investigated the model performance over the Greenland ice sheet and found that the model tends to overestimate the turbulent exchange in the surface layer in very stable conditions. King (1990) found that the Monin–Obukhov similarity theory might not be applicable to conditions at Halley. In this paper, we will focus on the ability of the model to simulate Antarctic katabatic winds and some closely related variables, such as sea level pressure, surface temperature, and wind directional constancy. A climate run, performed with the same model, enables us to cast a look at the climate sensitivity of Antarctic katabatic winds (section 4). In the next section, we give a short outline of the model physics and the set up of the climate experiment.

2. Model and experiments

The ECHAM-3 GCM has been developed at the Max-Planck Institute for Meteorology in Hamburg, Germany. The model has evolved from the spectral numerical weather forecasting model of the ECMWF in Reading, United Kingdom (hence the starting letters EC), and has been modified in Hamburg to make it suitable for climate applications (Roeckner et al. 1992). Prognostic variables are vorticity, divergence, temperature, surface pressure, water

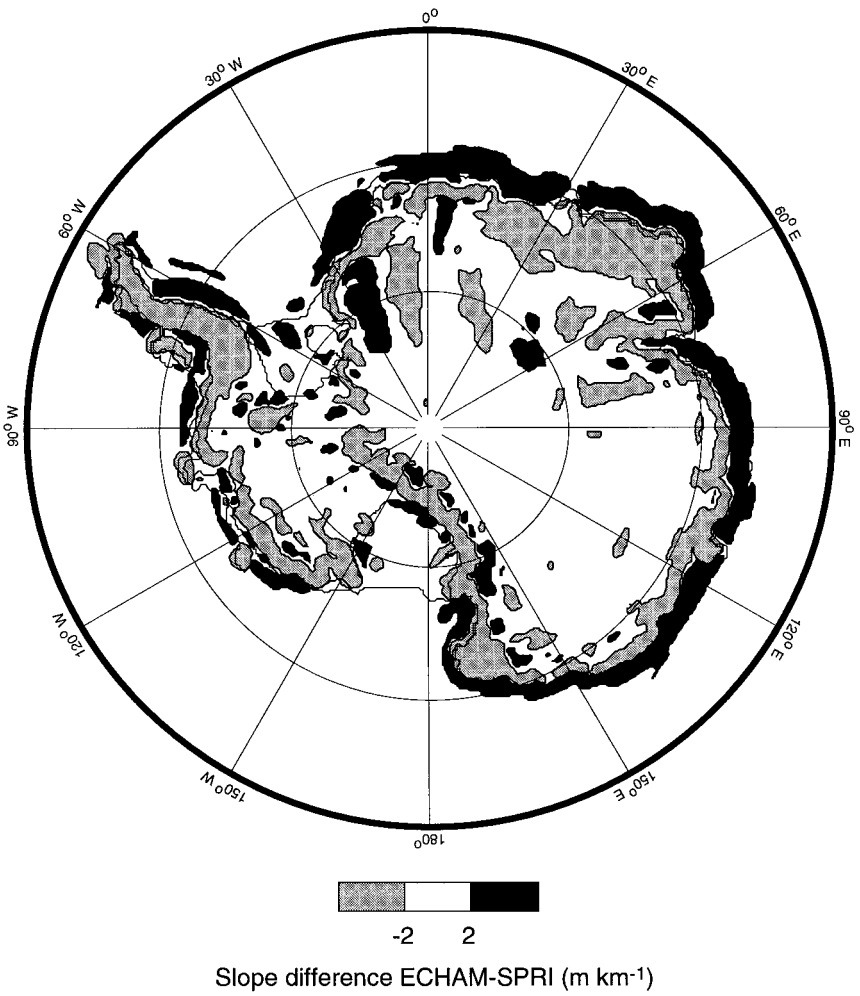

FIG. 2. Difference in surface slope between ECHAM and SPRI data. Areas where ECHAM − SPRI < -2 m km^{-1} are light shaded, ECHAM − SPRI > 2 m km^{-1} dark shaded.

vapor, and cloud water. The model equations are solved on 19 vertical levels using the spectral transform method with triangular truncation. The radiation scheme is based on a two-stream approximation of the radiative transfer equation with four spectral intervals in the solar part and six intervals in the longwave part of the spectrum (Hense et al. 1982). Gaseous absorption due to water vapor, carbon dioxide, and ozone is taken into account as well as scattering and absorption due to aerosols and clouds. The cloud optical properties are parameterized in terms of cloud water content (Stephens 1978). The cloud water content is obtained from the respective budget equation, including sources and sinks due to condensation, evaporation, and precipitation formation by coalescence of cloud droplets, and sedimentation of ice crystals (Sundquist 1978; Roeckner et al. 1991). Subgrid-scale condensation and cloud formation is taken into account by specifying appropriate thresholds of relative humidity depending on height and stability. A mass flux scheme is used for the parameterization of cumulus convection, which comprises the effect of deep, shallow, and midlevel convection on the budget of heat, water vapor, and momentum (Tiedke 1989). The vertical turbulent transfer of momentum, heat, water vapor, and cloud water is based on the Monin–Obukhov similarity theory for the surface layer and on the eddy diffusivity approach above the surface layer (Louis 1979). The land-surface scheme includes the budgets of heat and water in the soil, snow over land, and the heat budget of glaciers and sea ice (Duemenil and Todini 1992). The heat transfer equation is solved in a five-layer model assuming vanishing heat flux at the bottom. Vegetation effects, such as the interception of rain and snow in the canopy and the stomatal control of evapotranspiration, are parameterized in a highly idealized way.

With the ECHAM-3 model, simulations at high horizontal resolution (T106, truncation at wavelength 106; i.e., the smallest resolved wavelength is 3.4°) of present and future climates have been performed at the Swiss Scientific Computing Center (CSCS) in a joint project between the Max-Planck Institute for Meteorology, Hamburg, and the

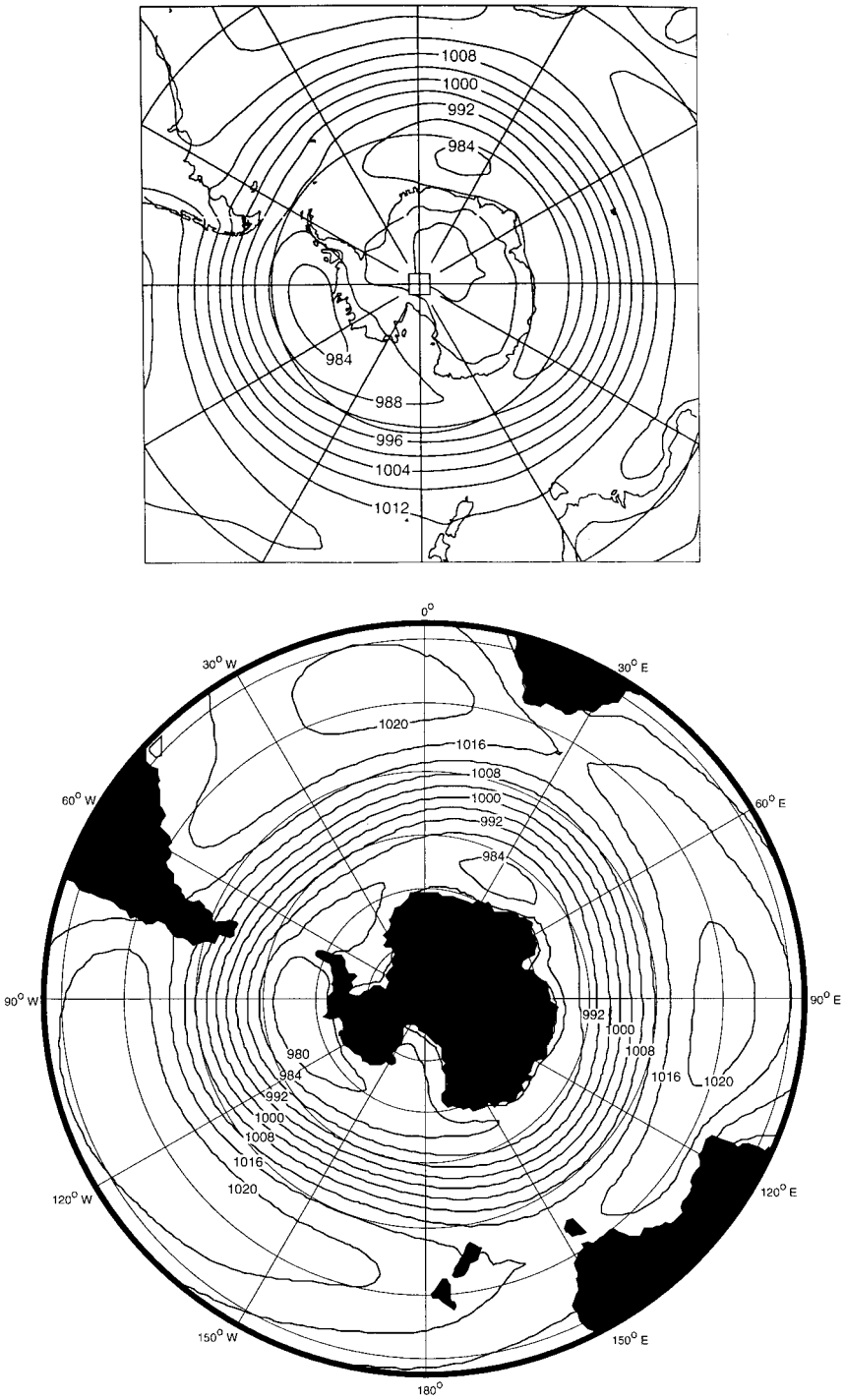

FIG. 3. Observed (a) and modeled (b) average summer (DJF) sea level pressure distribution; observed (c) and modeled (d) average winter (JJA) sea level pressure distribution. The observations are 10-yr mean distributions of UKMO data assimilation, taken from Connolley and Cattle (1994).

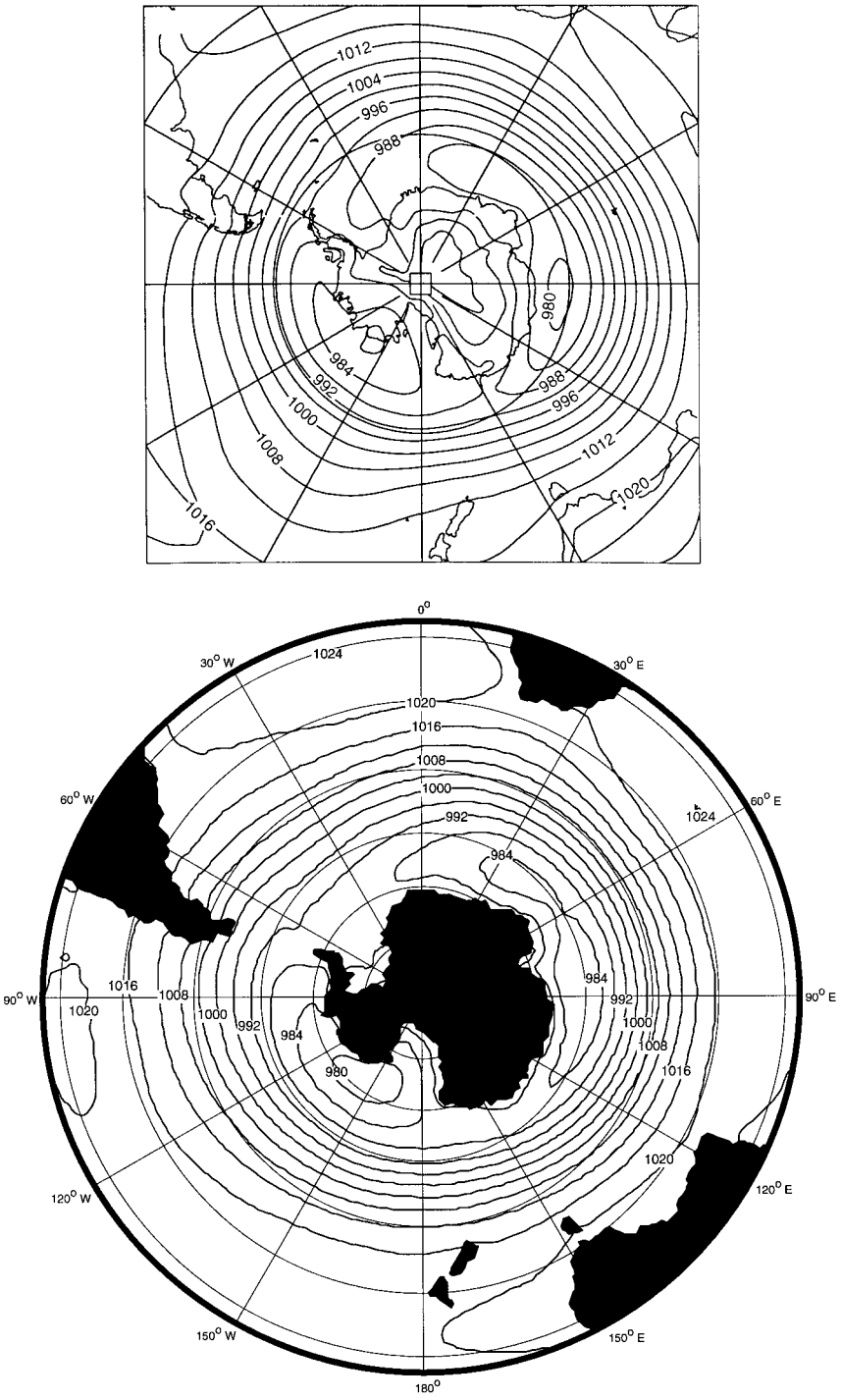

FIG. 3. (*Continued*)

Swiss Federal Institute of Technology, Zurich. The model formulation and parameters are identical for the different ECHAM-3 resolutions with two exceptions. The horizontal diffusion coefficients were set resolution dependent, such that the slope of the spectral kinetic energy comes close to observations. Furthermore, a rain efficiency parameter in the cloud scheme was set resolution dependent, which influences the cloud lifetime and, thereby, the associated planetary albedo, in order to match the global annual mean top of atmosphere radiative fluxes with satellite observations (Roeckner et al. 1992).

To simulate the present-day climate, the ECHAM3

GCM has been integrated at T106 resolution over 5½ yr (model time). In this control run, sea surface temperatures and sea ice were prescribed daily by linear interpolation between monthly mean climatologies from the Atmospheric Intercomparison Project (AMIP) sea surface temperature and sea-ice dataset (Gates 1992). The orography is based on mean terrain heights computed from the high-resolution (10′) U.S. Navy dataset. Five complete years of T106 simulation were used in the analysis. Since it is not feasible with today's supercomputing resources to run such a high-resolution GCM over several decades, as required in transient climatic change experiments, a ''time-slice'' experiment was performed. Thereby, the T106 atmospheric model has been run with prescribed boundary conditions of sea surface temperature and sea ice at the time of doubled carbon dioxide inferred from a low-resolution, fully coupled atmosphere–ocean transient experiment. The latter experiment has been performed at the Max-Planck Institute, where a T21 version of ECHAM, coupled to a dynamic ocean and sea-ice model, was integrated for 100 yr with a gradual increase of carbon dioxide according to Intergovernmental Panel on Climate Change (IPCC) scenario A (Cubasch et al. 1992). Changes in the sea surface temperature and sea ice projected by this coupled experiment, with respect to a coupled control run, were averaged over the period when the doubling of carbon dioxide is expected (2040–2050). These were then superimposed on the AMIP sea surface temperature and sea-ice dataset to serve as boundary conditions for the T106 run. Forced with these boundary conditions and a doubled carbon dioxide concentration, the T106 model was then integrated for 5½ yr to provide a climate change scenario of unprecedented high resolution.

3. Simulation of the present-day Antarctic climate

In this section we analyze the ability of ECHAM-3 T106 to simulate the present-day Antarctic climate. We use data from more than 30 manned stations and AWS to test the model results. Model output was interpolated to a 50 × 50 km grid, and the closest grid point that showed good altitude agreement with the station was selected to compare with observations. Figure 1 shows the location of the stations that were used, together with some of the main topographic features of Antarctica that are referred to in the text.

a. Topography and surface slope

The topography used in ECHAM-3 T106 is similar to that used in the ECMWF model and is based on the U.S. Navy dataset. Genthon and Braun (1995) made a comparison of this dataset with observations, and their main findings will be repeated here. Beside the effect of resolution, which tends to smooth out the topography of the Transantarctic Mountains and the Antarctic Peninsula, two areas with large anomalies show up: western Queen Maud Land is too high, by up to 1000 m in the model topography, while some areas in Enderby Land are up to 600 m too low. Of direct influence to the simulation of katabatic winds is the representation of the surface slope. Figure 2 shows the main differences in surface slope between ECHAM-3 and that derived from the Scott Polar Research Institute (SPRI) topography (Drewry 1983). In reality, the polar plateau quite suddenly drops to sea level with slopes of the order 0.1. By cutting off the higher wavenumbers, the model topography has an artificial extension to the north by as much as 1 grid point (≈100 km), both in East Antarctica and in the peninsula area. Because the model topography does not fall off quite so quickly toward the ocean, a large area bordering the coast suffers from slope underestimation (light gray shaded area in Fig. 2), while farther toward the north the surface slope is overestimated (dark gray shaded area). Nevertheless, the T106 topography is much more detailed than in most other climate simulations so far.

b. Sea level pressure and the circumpolar trough

Near-surface winds in the coastal area of Antarctica are modified by cyclones that originate from lower latitudes and migrate south-eastward along the coast. This cyclonic activity shows up in the pressure climatology as a belt of low pressure that surrounds the continent (the circumpolar trough or storm belt). Figure 3 compares the simulated summer [December–February (DJF)] and winter [June–August (JJA)] mean sea level pressure distribution with observations presented by Connolley and Cattle (1994), derived from 10 yr of UKMO (U.K. Meteorological Office) data assimilation. The modeled pressure fields show good agreement with the observations. For the Antarctic summer (Figs. 3a,b), the observations show the smallest values of closed contours of 984 hPa centered at 20° E (this simulation: 984 hPa, 30°E) and of 984 hPa centered at 105°W (simulation: 980 hPa, 105°W). The winter climatology (Figs. 3c,d) shows values of 984 hPa at 30°E (simulation: 984 hPa, 40°E), 980 hPa at 95°E (simulation: 984 hPa at 90°E), and 980 hPa at 140°W (simulation: 980 hPa at 140°W). As was also stated by Connolley and Cattle (1994), these differences are certainly smaller than the differences between some climatologies. For instance, the January sea level pressure distribution presented by Taljaard et al. (1969) shows additional pressure minima in the Bellingshausen and Weddell Seas in summer, while the low pressure center close to the Ross Sea is located at 160°W rather than at 140°W.

Figure 4a compares the modeled annual cycle of the zonally averaged depth of the circumpolar trough with observations presented by van Loon (1972), Xu et al. (1990), and the ECMWF analysis (1980–89), as presented by Tzeng et al. (1994). The amplitude of the semiannual oscillation is well simulated, with a secondary minimum in autumn, but the model lags the

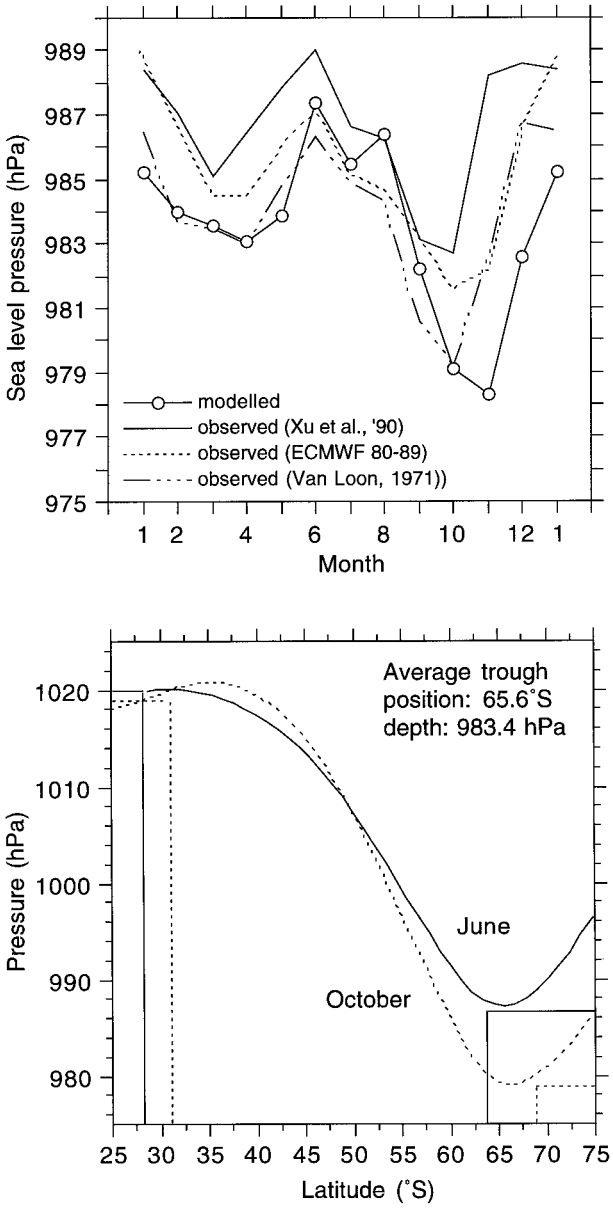

FIG. 4. (a) Modeled (dots) and observed (lines) annual cycle of the depth of the circumpolar low pressure belt. Observations are taken from Xu et al. (1990), Tzeng et al. (1994), and van Loon (1972). (b) Modeled meridional profiles of zonally averaged sea level pressure for June (solid line) and October (dashed line). Junctions of the straight lines indicate observations by van Loon (1972).

timing of the pressure rise in spring by 1 month. The modeled absolute values coincide with the lower range of the observations. Figure 4b presents the zonally averaged meridional profile of sea level pressure for 2 months, during which trough depth and location have extreme values, June and October. The straight lines in the figure correspond to observations presented by van Loon (1972). Although the pressure in the center of the trough compares well with these observations, the southward migration of the trough from June to October is limited to 1° in the model (from 65° to 66°S) while it is about 4 latitudinal degrees in the observations (from 64 to 68°S). This deficiency can be partly explained by the model topography that extends too far to the north, preventing low pressure areas to move farther southward.

The center pressure of the subtropical ridge (Fig. 4b) is overestimated by 2 hPa in October but well modeled in June. The position of the ridge is displaced 2° to the south in June and as much as 5° to the south in October, which is most probably due to model errors in the simulation of the (sub)tropical atmosphere. As a consequence, the modeled latitudinal pressure gradient from 35° to 65°S, which determines the strength of the midlatitude westerlies, is overestimated by as much as 30% in October. This can be traced back in Fig. 5, which compares the modeled annual cycle of zonally averaged geostrophic wind speed at sea level with observations presented by van Loon et al. (1971). The model clearly overestimates the strength of the midlatitude surface westerlies at 55° and 60°S, while the maxima in wind speed lag the observations by 1 month. The strength of the coastal easterlies and the disappearance of the semiannual oscillation at 70° are well represented. What are the consequences of all this for the capacity of the model to simulate the annual cycle of sea level pressure in the Antarctic coastal zone? Figure 6 shows the annual cycle of sea level pressure of four coastal stations around the continent [based on data compiled by Smith and Stearns (1993)] and compares it with model output at the nearest grid point. The modeled sea level pressure agrees, in general, within 5 hPa of the observed values. However, the lag of 1 month between model and observed pressure is also evident in these figures.

Summarizing this section, ECHAM-3 in T106 mode predicts the longitudinal and latitudinal position and depth of the circumpolar storm belt with fair accuracy. However, the seasonal latitudinal variation of the trough is suppressed and the position of the subtropical ridge is predicted several degrees too far south, which results in an overestimation of the midlatitude westerlies by as much as 30%. Moreover, the deepening of the trough from winter toward spring lags the observations by 1 month, which is reflected in the seasonal cycle of sea level pressure in the coastal areas of Antarctica. The present results, nevertheless, represent an improvement over earlier studies.

c. Near-surface temperature climate

Table 1 compares modeled and observed annual mean 2-m temperature at 31 stations in Antarctica (note that no corrections have been made to account for differences in station and model elevation). The stations have been grouped into seven climatological regions, based on elevation, mean temperature, and the shape of the annual temperature curve. The AWS data have been taken from Allison et al. (1993). For the other stations,

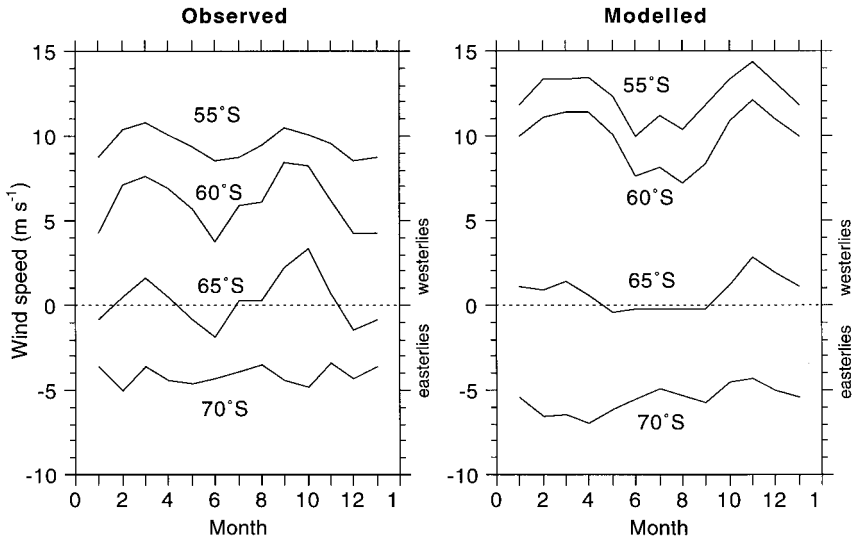

FIG. 5. Observed (van Loon et al. 1971) (left) and modeled (right) annual cycle of the zonal geostrophic wind speed, zonally averaged. Positive values indicate westerlies; negative values easterlies.

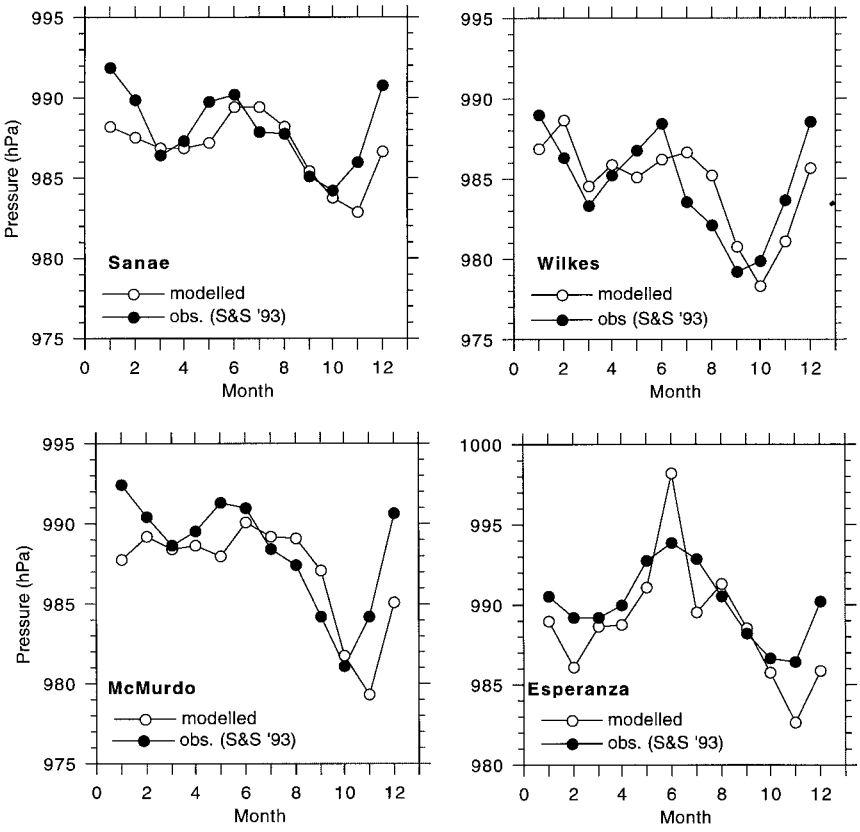

FIG. 6. Observed (black dots) and modeled (white dots) annual cycle of sea level pressure at four Antarctic stations. Abbreviated data source: S&S '93, Smith and Stearns (1993).

TABLE 1. Position, elevation, annual mean 2-m temperature, and 10-m wind speed at selected Antarctic stations, observed (obs) and modeled (mod). Elevations are above mean sea levels. AWS indicates Automatic Weather Station. The data have been grouped into seven climatological regions. Data were taken from Allison et al. (1993), Smith and Stearns (1993), and Schwerdtfeger (1970).

	Position		Elevation (m)		T_{2m} (°C)		V_{10m} (m s^{-1})	
Region/station	Lat °S	Long °	Obs	Mod	Obs	Mod	Obs	Mod
I. Plateau								
South Pole	90.0	—	2800	2889	−49.3	−48.6	6.2	6.0
Plateau	79.2	40.5 E	3625	3463	−56.4	−53.3	4.9	6.0
Vostok	78.5	106.9 E	3488	3483	−55.4	−53.9	5.1	6.4
GC41 AWS	71.6	111.3 E	2759	2747	−43.6	−46.0	6.4	8.0
Dome C AWS	74.5	123.0 E	3280	3047	−50.6	−51.6	3.2	5.5
D80 AWS	70.0	134.7 E	2500	2491	−40.6	−39.2	6.2	9.3
II. Katabatic East Antarctica								
Mizuho	70.7	44.3 E	2230	2154	−32.3	−32.7	10.0	12.0
GE03 AWS	68.7	61.1 E	1833	1773	−28.7	−27.5	11.1	9.6
Pionerskaya	69.7	95.5 E	2740	2769	−38.0	−39.0	10.6	10.3
GF08 AWS	68.5	102.2 E	2120	2043	−31.2	−33.3	13.8	12.4
A028 AWS	68.4	112.2 E	1625	1612	−26.8	−27.2	12.1	12.1
D47 AWS	67.4	138.7 E	1560	1651	−24.7	−26.4	10.9	10.7
III. Coastal East Antarctica								
Novolazarevskaya	70.8	11.8 E	99	153	−10.4	−14.0	10.3	8.1
Syowa	69.0	39.6 E	21	59	−10.5	−12.2	5.9	8.2
Molodezhnaya	67.7	45.9 E	40	69	−11.0	−12.2	10.3	7.5
Mawson	67.6	62.9 E	16	23	−11.3	−13.9	10.9	8.1
Davis	68.6	78.0 E	13	5	−10.3	−12.6	4.9	6.2
Mirny	66.6	93.0 E	30	19	−11.3	−10.8	11.5	8.6
Casey	66.3	110.5 E	15	43	−9.2	−12.5	6.9	8.9
D10 AWS	66.7	139.8 E	240	171	−12.8	−13.9	8.4	9.2
Dumont d'Urville	66.7	140.0 E	43	20	−10.7	−12.6	10.9	8.3
IV. Ross Ice Shelf								
Hallett	72.3	170.3 W	5	10	−15.3	−15.9	3.6	8.1
McMurdo	77.9	166.7 E	24	35	−17.2	−16.7	6.5	7.2
Gill AWS	80.0	178.6 W	55	13	−28.5	−17.2	4.0	6.4
V. West Antarctica								
Byrd	80.0	119.5 W	1515	1594	−27.7	−26.9	8.6	9.3
Eights	75.5	77.2 W	420	475	−26.0	−19.9	5.4	6.6
VI. Peninsula								
Esperanza	63.4	57.0 W	8	60	−5.6	−5.2	9.2	9.3
Orcadas	60.7	44.7 W	6	9	−3.8	−3.1	5.0	9.8
VII. Weddell Sea, east coast								
Belgrano	78.0	38.8 W	32	62	−22.3	−14.6	5.5	6.4
Halley	75.5	26.7 W	32	17	−18.4	−12.6	4.8	7.5
Sanae	70.3	2.4 W	52	4	−17.1	−12.6	7.4	7.7

temperature data from Schwerdtfeger (1984) and Smith and Stearns (1993) were used. The latter dataset covers the period from the International Geophysical Year (1957) to, on average, 1988. Ohmura et al. (1996) compared the modeled distribution of annual mean surface temperature to the map of Giovinetto et al. (1990) and found that the agreement, with exception of the ice shelves, was satisfactory. Here we will restrict ourselves to a direct comparison with station data.

For the six stations on the polar plateau in East Antarctica (region I), where the surface elevation exceeds 2500 m above mean sea level (MSL) and the annual mean temperature is lower than −40°C, the modeled and observed temperature generally agree within 2–3 K, the mean difference being 0.6 K. This is a good result, given the strong surface inversion on the plateau, which can reach a strength of 20–25 K over a 1000-m deep layer during the winter (Phillpot and Zillman 1970; Schwerdtfeger 1984). The model performance in the katabatic wind region in East Antarctica (region II) is also good, with differences between simulation and observation that are generally within 2 K. Annual mean temperatures in the coastal area of East Antarctica (region III) are on average too cold by 1.9 K, which is caused by underestimated winter temperatures. This is probably due to the overestimated sea ice thickness, which is prescribed in the model as alternating rows of 1 and 2 m thick, to account schematically for the occurrence of young and multiyear sea ice. Moreover, it is well known that sea ice is generally intersected with leads, which add additional heat to the atmosphere. These are not accounted for in the present model, which

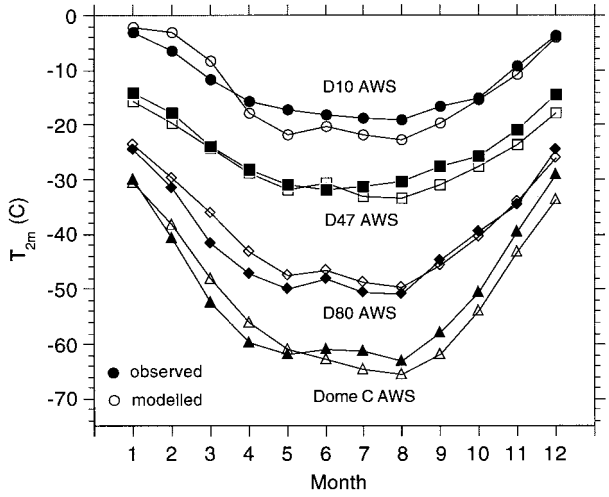

FIG. 7. Observed (black symbols) and modeled (white symbols) annual cycle of near-surface temperature at four Antarctic AWSs in Adélie Land. Observations from Allison et al. (1993).

could lead to an overestimation of surface pressure and an underestimation of temperature and moisture content over the sea ice (Simmonds and Budd 1991; Walsh and McGregor 1996). The influence of sea-ice characteristics on the near-coastal temperatures was also mentioned by Tzeng et al. (1994), who found the same problems in CCM2, in which sea is prescribed as a uniform 2-m thick ice layer.

A serious flaw in the model is the treatment of ice shelves as sea ice rather than land ice. The latter would be more appropriate, because the thickness of the ice shelves of 200–1000 m assures that the heat flux from the ocean plays a minor role in the surface energy budget. In the present model, the heat flux from the ocean to the surface of the ice shelf can be as large as 50 W m^{-2} in the winter months, thereby largely compensating for the loss of longwave radiation toward the atmosphere. This results in a 10–20-K overestimation of the surface temperature in winter. In Table 1, the model error is most apparent for the stations that are situated on large ice shelves, like Gill AWS (region IV, Ross Ice Shelf, temperature 11.3 K too high), Eights (region V,

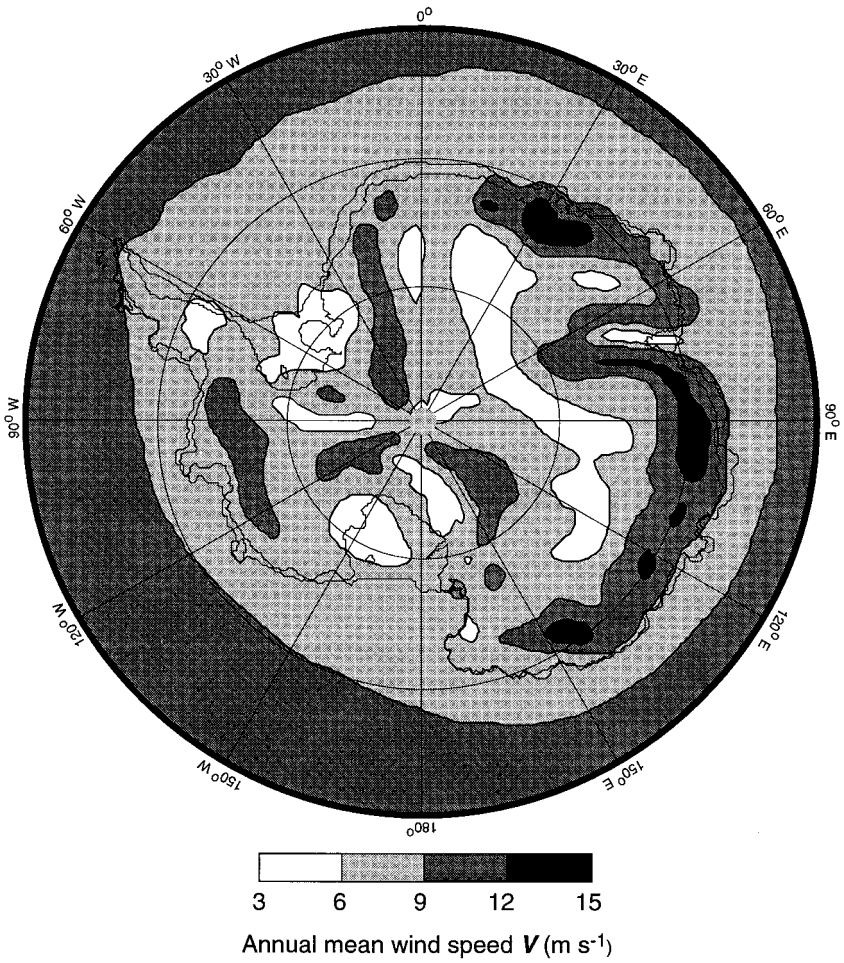

FIG. 8. Modeled distribution of annual mean 10-m wind speed.

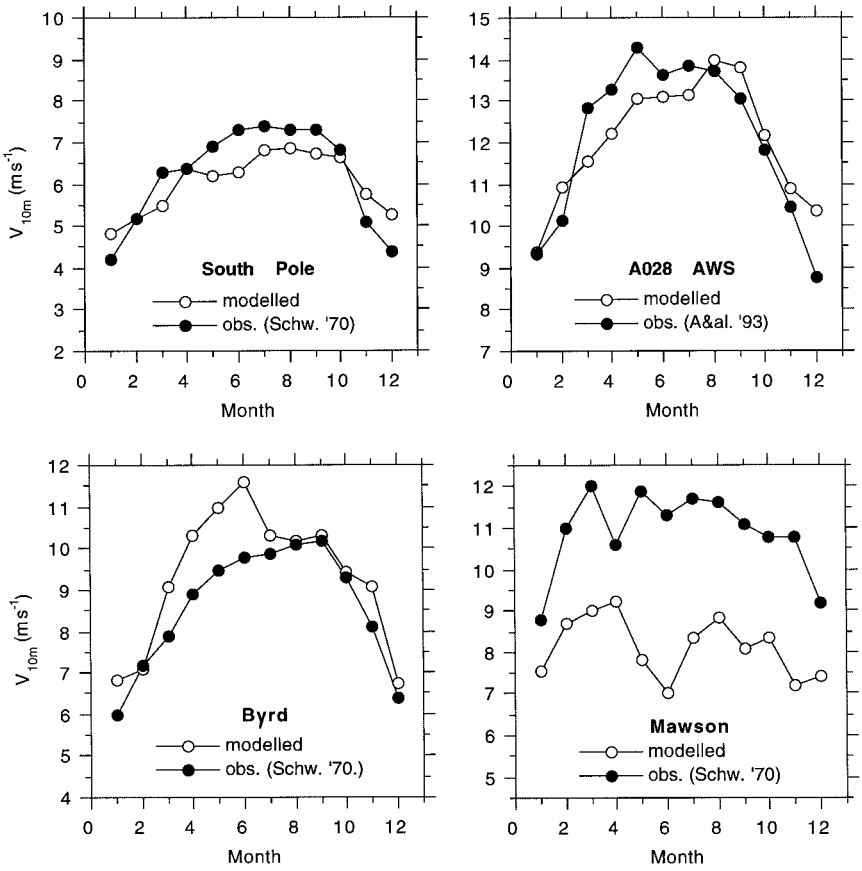

FIG. 9. Observed (black dots) and modeled (white dots) annual cycle of 10-m wind speed at four Antarctic stations. Abbreviated data sources: Schw. '70, Schwerdtfeger (1970); A&al. '93, Allison et al. (1993).

in the vicinity of the Filchner Ronne Ice Shelf, 6.1 K), Belgrano (region VII, Filchner Ronne Ice Shelf, 7.7 K), Halley (region VII, on the eastern coast of the Weddell Sea on the Brunt Ice Shelf, 5.8 K), and Sanae (region VII, Fimbul Ice Shelf, 4.5 K). Annual mean temperatures of the two peninsula stations (region VI) are well modeled.

The ability of the model to simulate the annual temperature cycle in different climate zones ranging from the East Antarctic plateau to the coast is illustrated for an array of AWS in Adélie Land (Fig. 7), for which the observations have been taken from Allison et al. (1993). In general, the decrease of the amplitude in the annual temperature cycle toward the coast is well simulated. Winter temperatures at the coastal station D10 AWS are modeled 3–4 K too low, and the autumn cooling on the plateau (D80 AWS, Dome C AWS) is not fast enough, especially from February to March. A peculiar feature of the annual temperature cycle in certain areas of Antarctica is the reversal of seasonal cooling, that is, the increase of temperature from May to June. Van Loon (1967) showed that this phenomenon can be explained by an amplification of the Rossby waves in the Indian and Pacific Oceans from April to June, which increases the meridional exchange of air. This results in increased warm air advection toward the Pacific and Indian sectors of Antarctica. He showed that this phenomenon can be traced back in the temperature records of stations where a significant inversion develops during the winter, that is, on the plateau, in the katabatic wind region, and on ice shelf stations. As can be seen in Fig. 7, the observations show a temperature reversal at D80 and Dome C AWS, while the model predicts a reversal at the stations D10, D47, and D80 AWS. Apparently, the model is capable of reproducing the hemispheric-scale mechanisms that are associated with the reversal of seasonal cooling, that is, the amplification of the Rossby waves toward the winter, but fails to advect the warm air far enough inland

d. Near-surface wind climate

Table 1 compares modeled annual mean 10-m wind speed with observations at several stations in Antarctica. Most wind speed data are taken from Schwerdtfeger (1970), which are thus compiled from a considerably shorter averaging period than most of the temperature data in the previous section. It should also be borne in

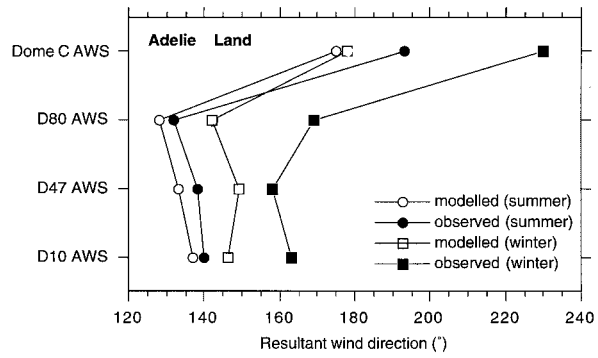

FIG. 10. Observed (black symbols) and modeled (white symbols) resultant wind direction at four AWS in Adélie Land. Squares denote winter (JJA) and circles summer (DJF) wind directions. Observations from Kodama and Wendler (1986).

mind that wind speed at the AWS sites are usually measured at 3 m above the surface, compared to 10 m at most manned stations and in the model. For instance, assuming a well-mixed (neutral) surface layer and a surface roughness of 1 mm, AWS wind speed data in Table 1 should be multiplied by a factor 1.15 to obtain approximate 10-m values.

The modeled wind speed on the plateau (region I) is generally too high, especially at D80 AWS. However, if we do not take this station into account and correct for the lower measurement level at the other AWS sites, the mean difference between observations and model on the plateau is only 1 m s^{-1}. The lowest wind speed is correctly modeled for Dome C AWS, which is currently the station with the lowest annual mean wind speed on the continent (Wendler and Kodama 1984). The model performance in the katabatic wind region in East Antarctica (region II) is good, and modeled wind speeds are generally within 2 m s^{-1} of the observations. The highest wind speed is correctly modeled for GF08 AWS. In the coastal areas of East Antarctica (region III), the model generally underpredicts the wind speed at stations that are influenced by katabatic winds from the plateau (i.e., Novolazerevskaya, Molodezhnaya, Mawson, Mirny, and Dumont d'Urville) and overpredicts it at stations where relatively low wind speeds are observed (i.e., Syowa, Davis, and Casey). This is probably a result of the local topographical conditions in the coastal zone that are not represented in the model topography and the smoothed representation of the ice sheet slope (Fig. 2). The low wind speeds observed at Hallett (region IV) and Orcadas (region VI) are most probably a result of the sheltered position of these stations and should not be considered representative for a larger area (Mather and Miller 1967).

Figure 8 shows the modeled distribution of annual mean 10-m wind speed. Many characteristics of the Antarctic wind climate are simulated by the model. Surrounding the continent, the belt with strong midlatitude westerlies has wind speeds of typically 9–10 m s^{-1}. Over the steep slopes of East Antarctica, the annual mean wind speed generally is between 9 and 12 m s^{-1}, and several areas with annual mean wind speeds exceeding 12 m s^{-1} are modeled, the maxima amounting to 14 m s^{-1}. In the absence of a significant surface slope, such as on the Ross Ice Shelf, the Filchner–Ronne Ice Shelf, the Amery Ice Shelf, and the domes of the ice sheet, gravity-driven winds are weak and the annual mean wind speed is generally lower than 6 m s^{-1}. An area with low wind speeds is also modeled in the middle of the Antarctic Peninsula at 70°W, but no data are available to confirm this. The same is valid for the area with low wind speeds that is predicted on the plateau southwest of the Transantarctic Mountains bordering the Ross Ice Shelf.

The modeled wind speed distributions for winter and summer months (not shown) are qualitatively similar to the yearly distribution, but wintertime winds are generally 15% stronger than the annual mean, and those during summer are 20% weaker. The wintertime simulations show maximum monthly mean wind speeds in July of 16 m s^{-1} in East Antarctica; this is lower than the model results presented by Parish and Bromwich (1991), but somewhat higher than the GCM-generated

TABLE 2. Observed and modeled directional constancy *dc* at selected Antarctic stations. Data from Schwerdtfeger (1984), Allison et al. (1993), and Breckenridge et al. (1993).

Region/station	Directional constancy *dc*	
	Obs	Mod
I. Plateau		
South Pole	0.79	0.80
Plateau	0.67	0.74
Vostok	0.81	0.80
Dome C AWS	0.52	0.69
D80 AWS	0.88	0.88
II. Katabatic East Antarctica		
Mizuho	0.96	0.94
Pionerskaya	0.92	0.93
GF08 AWS	0.99	0.94
A028 AWS	0.97	0.93
D47 AWS	0.93	0.91
III. Coastal East Antarctica		
Molodezhnaya	0.85	0.78
Mirny	0.90	0.60
Casey	0.61	0.83
D10 AWS	0.91	0.82
IV. Ross Ice Shelf		
Little America	0.48	0.41
Ferrell AWS	0.79	0.73
V. West Antarctica		
Byrd	0.86	0.89
VI. Peninsula		
Faraday	0.21	0.32
Orcadas	0.28	0.59
Matienzo	0.73	0.40
VII. Weddell Sea, east coast		
Halley	0.62	0.72

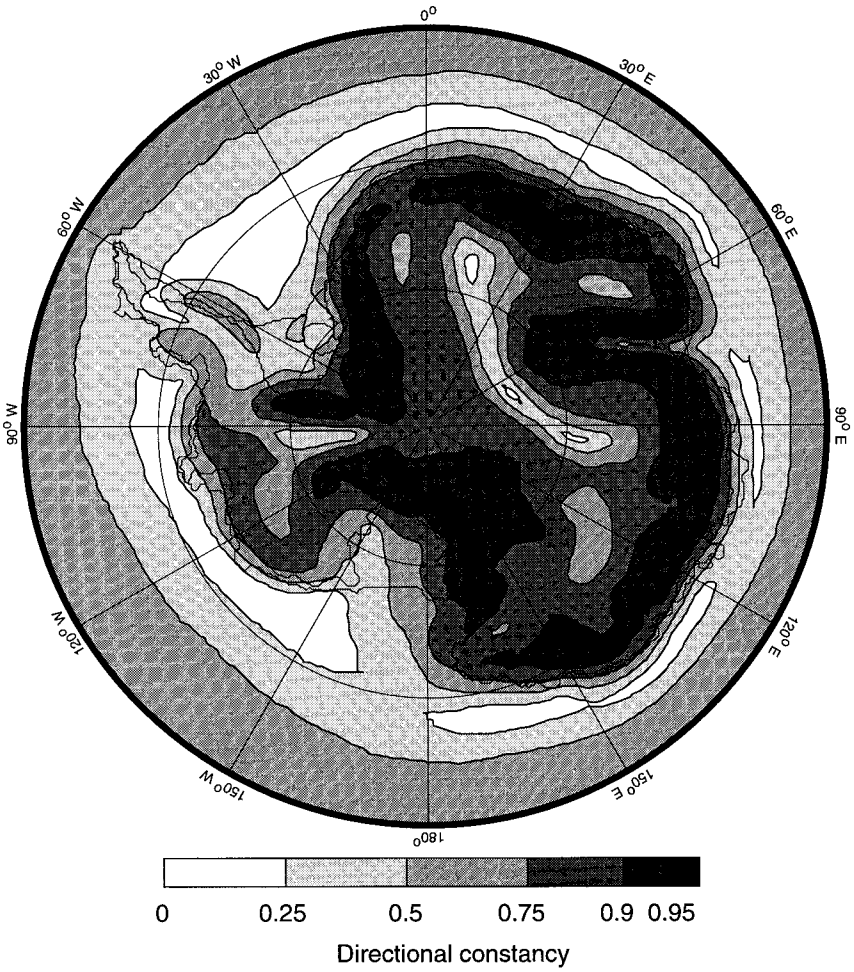

FIG. 11. Modeled distribution of annual mean directional constancy *dc*.

wind field of Tzeng et al. (1994), although the latter presented vector averages (which should be divided by the directional constancy to obtain mean absolute wind speed). Areas with exceptionally high annual mean wind speeds (such as in the coastal area of Adélie Land) coincide generally with places where the topography forces the gravity flow to converge, causing an additional acceleration (Parish and Bromwich 1987). However, this does not hold true for all areas. Although Allison et al. (1993) stated that the extremely high wind speed observed at GF08 AWS at 102°E is caused by the local topography, the present results suggest that comparably strong winds (i.e., >12 m s^{-1} annual mean) could also occur in a large area west of this station. It is suggested that the favorable climatological pressure gradient (Fig. 3) could considerably enhance the surface flow in some coastal areas (Murphy and Simmonds 1993).

Figure 9 shows modeled and observed annual cycle of wind speed at four stations in different climate zones. The model underestimates the strength of the wind in the coastal region of East Antarctica (region III, here represented by Mawson), but the performance on the plateau, in the katabatic wind region, and in West Antarctica is generally good. In agreement with observations, stronger winds are simulated in the winter in all regions. The largest amplitude of the annual cycle of wind speed, about 5 m s^{-1}, is found in the katabatic wind region, whereas the smallest amplitude, 2–3 m s^{-1}, is correctly simulated for coastal East Antarctica. In Figure 10 we compare the resultant wind direction, averaged for the summer (DJF) and winter (JJA) months with observations at several AWS in Adélie Land (Kodama and Wendler 1986). In summer, the wind direction is well predicted. The model winds have a larger downslope component during the winter months, but the difference with summer is not as large as in the observations. Except for Dome C AWS, the difference between model and observations in the katabatic wind zone are generally within 20°, which is acceptable.

In order to study persistent flow features, the directional constancy *dc* is a useful quantity. It is defined as the ratio magnitude of the mean vector wind to that of the mean wind speed; $dc = 1$ indicates that the wind is

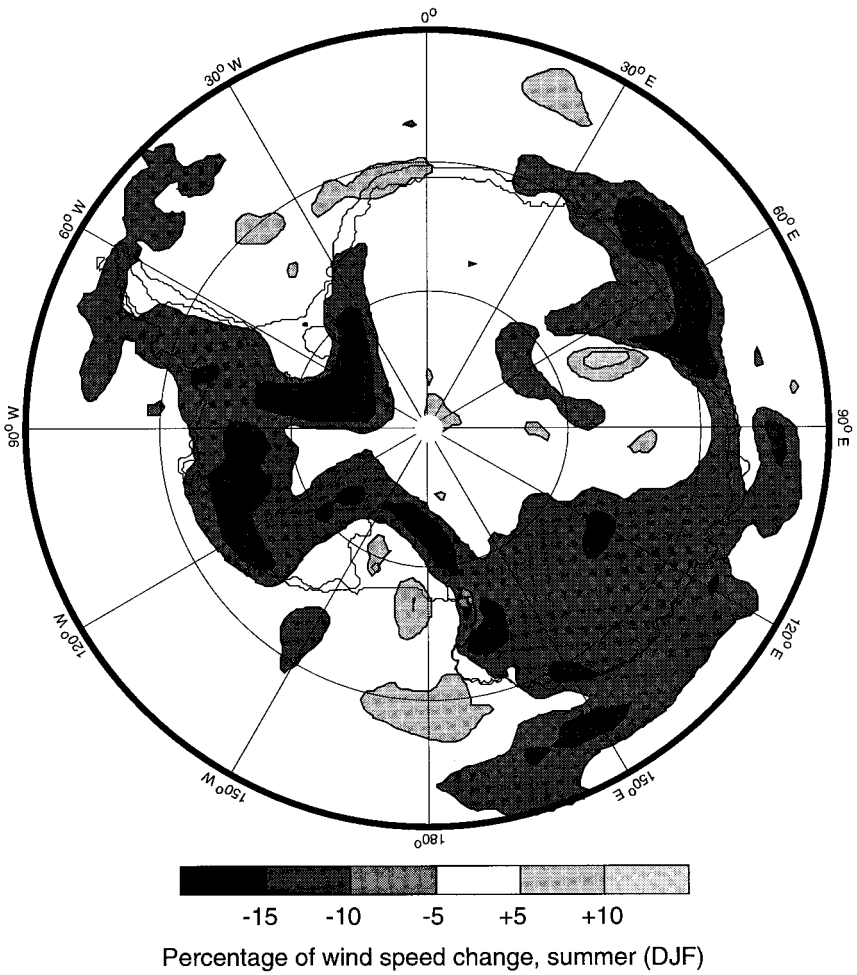

FIG. 12. Modeled relative change ($2 \times CO_2$–present) of 10-m wind speed for (a) summer months (DJF) and (b) winter months (JJA).

unidirectional, while $dc = 0$ indicates that the vector averaged wind speed equals zero, that is, winds tend to blow from opposite or random directions. In Table 2, modeled and observed annual mean *dc* are compared at several stations. The model is able to distinguish between the very persistent katabatic winds in East Antarctica (region II, $dc > 0.9$) and the winds on the plateau (region I, $dc = 0.7$–0.8), which were indicated as ''inversion winds'' by Schwerdtfeger (1984). The modeled values for the other locations are also in fair agreement with the observations, with the exception of some stations in the coastal area of East Antarctica (region III), where the gradients of *dc* are very large.

Figure 11 presents the modeled distribution of annual mean *dc*. Several interesting features can be found in this figure: in the belt with midlatitude westerlies, the directional constancy is modestly high ($dc = 0.5$–0.75). Apparently, the frequent passage of low pressure systems prevents higher values of *dc*, but no data are available to check this assumption. In the area close to the continent where both westerlies and easterlies occur (depending on the exact location of the circumpolar trough), we find a distinct minimum in directional constancy ($dc < 0.25$). Over the steep slopes of the ice sheet of East Antarctica, katabatic winds are characterised by very high values of *dc*. Over the plateau, where surface slopes are more gentle, we see a gradual decrease of *dc* in response to the smaller influence of gravity on the near-surface flow. On the domes of the ice sheet, where gravity flow is absent, *dc* tends to become very low. Except for Dome C AWS (Table 2), no data are available for the domes in East Antarctica to verify these numbers. An area with very high values of *dc* is found on the plateau just southwest of the Transantarctic Mountains. However, this region is not exposed to strong katabatic winds but is, on the contrary, characterized by low annual wind speeds (Fig. 8). At present there is no clear explanation for neither the high value of *dc*, nor for the low wind speeds in this area.

Toward the western parts of the Filchner and Ross Ice Shelves, both the modeled wind speed and directional constancy increase (note the maximum in *dc* at

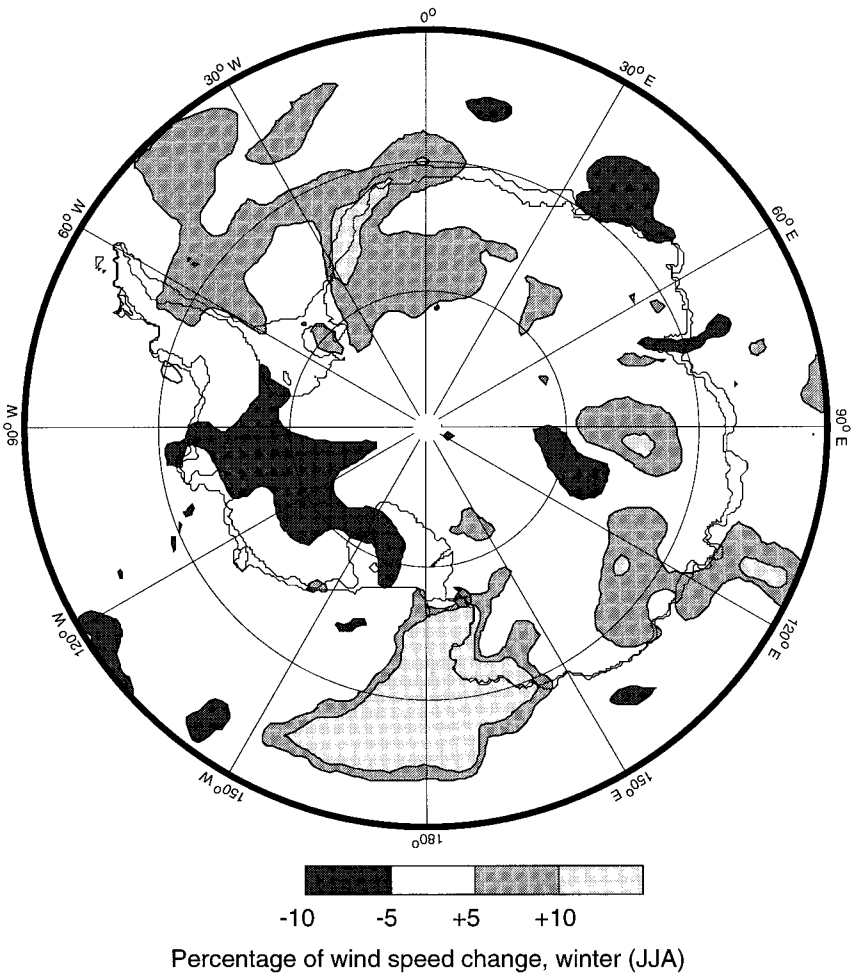

FIG. 12. (*Continued*)

the eastern border of the peninsula). At these locations, the piling up of relatively cold ice shelf air against the Antarctic Peninsula and the Transantarctic Mountains forces so-called barrier winds, that is, a strong and persistent jet that blows along the topography. This is a well-documented climatological feature of both ice shelves (Schwerdtfeger 1984). Along the Transantarctic Mountains and over the Ross Ice Shelf, barrier winds tend to destroy the surface inversion, causing large horizontal temperature gradients at the surface; compare for instance, the observed annual mean temperatures of McMurdo and Gill AWS in Table 1, both at the same elevation and latitude. The high values of *dc* that are modeled on the western part of the Ross Ice Shelf are confirmed by Breckenridge et al. (1993), who reported values of 0.76–0.84 for three AWSs close to the Transantarctic Mountains. One of these stations, Ferrell AWS, is included in Table 2. Barrier winds at the eastern side of the Antarctic Peninsula advect cold air from the south and are responsible for the relatively cold and windy climate of the Weddell Sea coast compared to the Bellingshausen Sea coast (Schwerdtfeger 1975). Matienzo, situated close to the northernmost tip of the Antarctic Peninsula (Fig. 1), is frequently under the influence of these barrier winds. The barrier wind signature in Fig. 11, however, clearly does not extend so far to the north, which is due to the artificial flattening of the model topography in places where the peninsula becomes very narrow. This enables the midlatitude westerlies in the model to penetrate too far to the south, dissipating the barrier wind, which result in low values of *dc* at the location of Matienzo (Table 2). In spite of this deficiency, it is encouraging that the model is, at least qualitatively, able to simulate these regional wind systems.

4. A preliminary note on the climate sensitivity of Antarctic katabatic winds

ECHAM-1, run in T21 resolution and coupled to a dynamic ocean and sea-ice model, was integrated for 100 yr with a gradual increase of carbon dioxide according to IPCC scenario A. Changes in sea surface temperature and sea ice cover then served as new bound-

ary conditions for a 5½-yr run in T106 mode (see section 2). The results of this run are used in this section to study the climate sensitivity of Antarctic katabatic winds. Although ECHAM-3 in T106 mode is well able to simulate the modern Antarctic climate, as was demonstrated in the previous sections, its ability to predict the future Antarctic climate depends on the accuracy of the boundary conditions produced by its low-resolution counterpart. The latter are, of course, hard to check. Therefore, the results presented in this section on the climate sensitivity of Antarctic katabatic winds should be regarded as preliminary.

In a $2 \times CO_2$ climate one would expect a warming of the surface due to a decrease in the longwave radiation loss, and hence a weakening of the surface inversion. This then might be expected to weaken the katabatic winds. However, with the decrease of near-surface static stability, we also expect an increase of the exchange between free atmosphere and boundary layer air, which could lead to either an increase or a decrease of the near-surface flow. The sensitivity of near-surface winds to geostrophic winds above the boundary layer is especially large in the short Antarctic summer, when the surface inversion is generally weak (Kodama et al. 1989; van den Broeke and Bintanja 1995b). Thus, stated in a qualitative manner, it depends on the strength and direction of the upper air winds in relation to the strength and direction of the katabatic flow how surface winds react to a change of the temperature inversion. Figures 12a,b show the change of near-surface wind speed between the $2 \times CO_2$ and present climate runs for summer (DJF) and winter (JJA). Surprisingly, the changes in the different seasons have opposite signs. During summer, a decrease of up to 15% of the wind speed is observed in large parts of the katabatic wind zone, while wintertime katabatic winds show local increases of up to 10%. As a result, the annual mean wind speed remains generally within 10% of its present value, showing a slight increase over the plateau and a decrease in the katabatic wind zone. In all regions, however, the amplitude of the annual cycle increases. Possible causes of this behavior will be discussed next.

a. Summer changes

It is found that the temperature–albedo feedback plays a decisive role in the destruction of the summertime surface inversion in the $2 \times CO_2$ climate, which causes the decrease of katabatic winds displayed in Fig. 12a. In ECHAM-3, the surface albedo α over snow is made a function of surface temperature, in line with observations by Robock (1980): $\alpha = \alpha_{\max} - (\alpha_{\max} - \alpha_{\min})(T_s - T_{\min})/(T_{\max} - T_{\min})$, where α_{max} and α_{min} denote the values that are used for surface temperatures below T_{min} and above T_{max}, respectively. In between these values, the albedo is prescribed to vary linearly with temperature. Here, T_{min} and T_{max} are set at -10°C and the melting point of snow, 0°C, both for sea and land ice. For sea ice, the values of α_{max} and α_{min} are set to 0.5 and 0.75, according to Robock (1980). For land ice surfaces, these values are 0.6 and 0.8, according to Kukla and Robinson (1980).

The inclusion of this simple parameterization of the temperature–albedo feedback in ECHAM-3 has important implications for the surface energy balance in the $2 \times CO_2$ climate. The difference of surface albedo between the two climate runs is presented in Fig. 13. Comparing Figs. 12a and 13, we see that areas where temperatures have increased above -10°C, and hence the surface albedo has decreased, generally coincide with the areas where summertime wind speeds have decreased, especially in West Antarctica. Although a decrease of 0.01–0.03 in surface albedo might not seem spectacular, for snow surfaces with a typical absorptivity of 0.20 it represents a 5%–15% increase of the amount of absorbed solar radiation, which is the largest positive term in the surface energy balance of dry Antarctic snow (Bintanja and Van den Broeke 1995). In relatively warm areas, where the -10°C isotherm is situated higher on the ice sheet, and therefore in regions where surface slopes are more gentle, the migration of the isotherms will cover a larger surface than in colder places for the same change in surface temperature. The decrease of surface albedo is, therefore, much more outspoken in West Antarctica than in East Antarctica, and the decrease of katabatic winds, consequently, larger. The low-lying and gently sloping ice streams in West Antarctica (bordering the Ross and Filchner Ronne ice shelves) are areas that are especially sensitive to these changes.

Large areas in East Antarctica experience a weakening of the wind without a significant change of the surface albedo, for example, Adélie Land and Enderby Land (Fig. 12a). Because the predicted changes in the sea level pressure field are small for the summer months, these changes must be associated with a change in horizontal temperature gradients in the lower troposphere (thermal wind effects).

b. Winter changes

For the winter months changes in albedo are small, but significant changes are found in the sea level pressure field. The zonally averaged pressure changes between the $2 \times CO_2$ run and the present climate are presented in Fig. 14, which shows a significant deepening of the circumpolar trough during winter, in contrast to the summer months. Figure 12b shows the change of wintertime wind speed, and Fig. 15 the aerial distribution of the change in sea level pressure. In some areas we find that the deepening of the circumpolar through is locally enhanced by the removal of sea ice in the $2 \times CO_2$ run (indicated by the dotted areas in Fig. 15). The magnitude of maximum pressure falls (3–7 hPa) is similar to that found by Mitchell and Senior (1989), who used a GCM to investigate

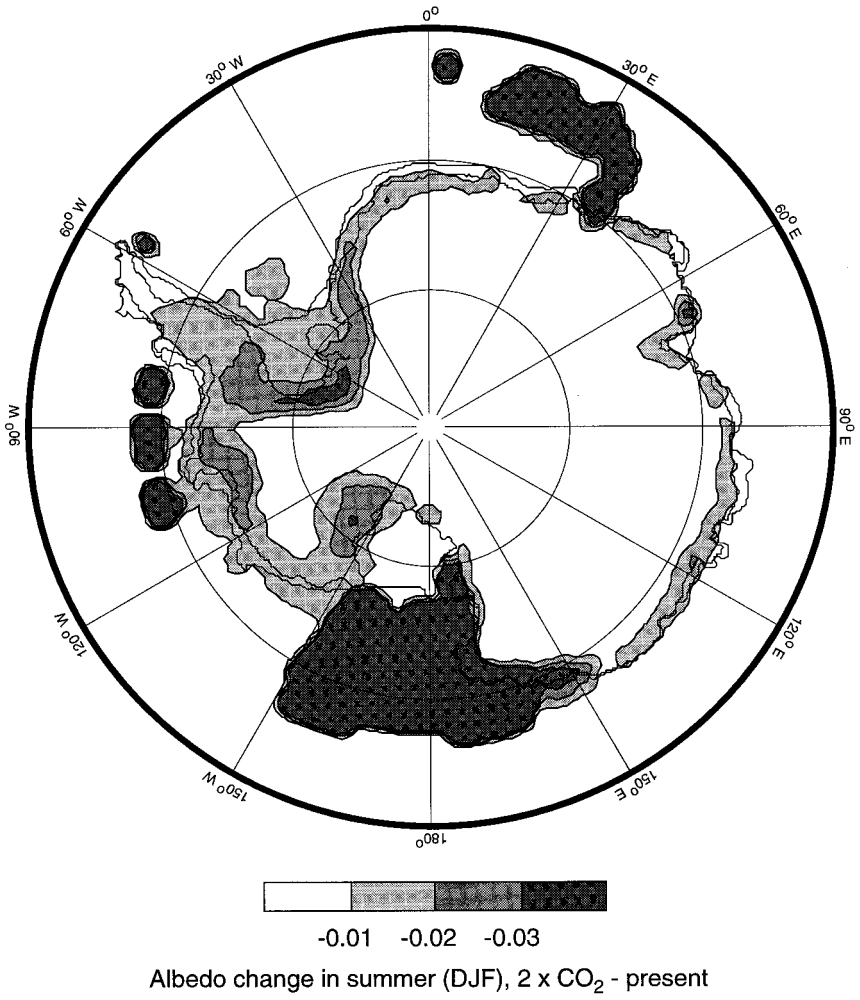

FIG. 13. Modeled change of surface albedo for the summer (DJF), 2 × CO_2–present. The pattern of summer albedo change shows essentially two effects in the 2 × CO_2 climate run. The first is the removal of sea ice at some places, leading to a dramatic drop in albedo from the sea-ice value (0.5–0.75) to that of sea water (0.065). These changes are visible as dark blobs. The second effect, which is of most interest here, are the more subtle changes that result from the temperature increase above the threshold for albedo changes (i.e., −10°C) over the coastal zone of the ice sheet.

the sensitivity of the Antarctic climate to the presence of sea ice. However, the pressure fall in the Weddell Sea is not connected to changes in sea ice cover, but indicates the more frequent transport of depressions across the Antarctic Peninsula owing to the stronger westerlies. The increase of wintertime near-surface wind speeds, as displayed in Fig. 12b, is clearly connected to areas where the decrease of sea level pressure is most pronounced, that is, in the eastern Weddell Sea coast, Wilkes Land, and the western Ross Sea coast. Here, the increase of easterly geostrophic winds above the boundary layer more than compensate for the decrease of the katabatic component of the near-surface flow.

5. Summary and conclusions

The ECHAM-3 T106 GCM simulates many important characteristics of the Antarctic climate, such as the position and seasonal cycle of the depth of the circumpolar trough, the midlatitude westerlies, the surface temperature, and near-surface wind field. Shortcomings of the model simulations are the treatment of the ice shelves, the suppressed annual cycle of the location of the circumpolar trough, and the latitudinal position of the subtropical ridge, which results in an overestimation of the strength of the westerlies. Moreover, the sea-ice parameterization and smoothing of the steep marginal ice slopes in the model topography lead to an underestimation of winter temperatures and wind speeds in the

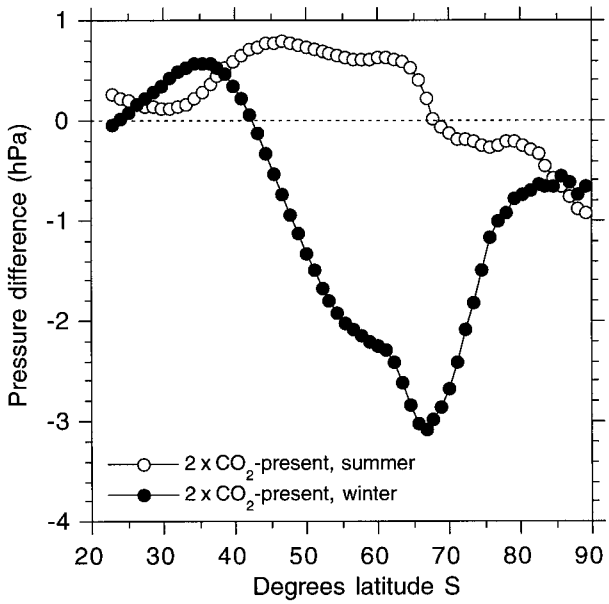

FIG. 14. Modeled change of zonally averaged sea level pressure, $2 \times CO_2$–present, for summer months (white dots) and winter months (black dots).

coastal areas. Nevertheless, the simulated synoptic and near-surface climates over Antarctica show considerable improvement over earlier simulations.

We studied the climate sensitivity of the near-surface winds over Antarctica, using output of a climate run that was performed with the same model, following the IPCC doubled CO_2 scenario A. We found that the sensitivity of the Antarctic near-surface airflow to this forcing is relatively small, the annual mean wind speed remaining within 10% of its present value. However, the response varied strongly between the summer (DJF) and winter (JJA) months, a result of the combined effects of changes in the surface temperature inversion and the strength and direction of the large-scale flow. The main findings are as follow:

- In summer, the temperature-dependent albedo parameterization causes an increase of the absorption of solar radiation at the surface in low-lying areas, especially in West Antarctica. Consequently, the strength of the surface inversion decreases. Because no significant changes occur in the geostrophic winds above the ABL, near-surface winds in the coastal areas decrease by as much as 15%.
- During the winter months, the model predicts a significant deepening of the circumpolar low pressure belt, which is locally enhanced by the removal of sea

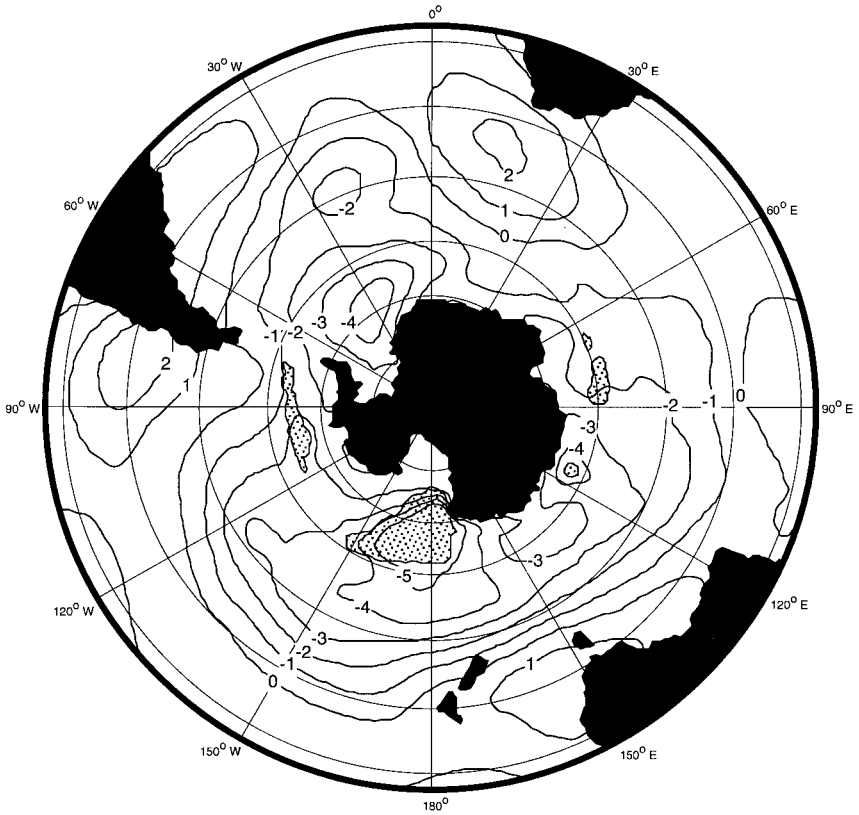

FIG. 15. Modeled change of sea level pressure for the winter (JJA), $2 \times CO_2$–present. Dotted areas indicate where sea ice has been removed in the $2 \times CO_2$ climate.

ice. The associated increase of the synoptic pressure gradient compensates for the decrease of the katabatic component, and near-surface wind speeds are found to increase by as much as 10% in areas where the pressure falls are most pronounced.

Because the processes that appear to be important for the climate sensitivity of Antarctic katabatic winds, like the dynamic sea-ice distribution and the temperature–albedo feedback, are modeled in a highly idealized way, the results of the $2 \times CO_2$ climate run should be regarded as preliminary.

Acknowledgments. We thank the Swiss Scientific Computing Center (CSCS) for generously providing the computer resources for the high-resolution simulations, and Prof. Bengtsson and U. Schlese from the Max-Planck Institute in Hamburg for their support.

REFERENCES

Allison, I., G. Wendler, and U. Radok, 1993: Climatology of the east Antarctic ice sheet (100°E to 140°E) derived from automatic weather stations. *J. Geophys. Res.,* **98** (D5), 8815–8823.

Bintanja, R., and M. R. van den Broeke, 1995: The surface energy balance of Antarctic snow and blue ice. *J. Appl. Meteor.,* **34,** 902–926.

Breckenridge, C. J., U. Radok, C. R. Stearns, and D. H. Bromwich, 1993: Katabatic winds along the Transantarctic Mountains. *Antarctic Meteorology and Climatology, Studies Based on Automatic Weather Stations,* D. H. Bromwich and C. R. Stearns, Eds., Antarctic Research Series, Vol. 61, Amer. Geophys. Union, 69–92.

Connolley, W. M., and H. Cattle, 1994: The Antarctic climate of the UKMO Unified Model. *Antarct. Sci.,* **6** (1), 115–122.

Cubasch, U., K. Hasselmann, H. Hoeck, E. Maier-Reimer, U. Mikolajewicz, B. D. Santer, and R. Sausen, 1992: Time-dependent greenhouse warming computations with a coupled ocean–atmosphere model. *Climate Dyn.,* **8,** 55–69.

Drewry, D. J., 1983: Antarctica: Glaciological and geophysical folio. Scott Polar Research Institute.

Duemenil, L., and E. Todini, 1992: A rainfall runoff scheme for use in the Hamburg climate model. *Advances in Numerical Hydrology. A Tribute of James Dooge,* J. P. O'Kane, Ed., European Geophysical Society Series on Hydrological Sciences, Vol. 1, Elsevier Science.

Gallée, H., 1995: Simulation of the mesocyclonic activity in the Ross Sea, Antarctica. *Mon. Wea. Rev.,* **123,** 2051–2069.

——, P. Pettré, and G. Schayes, 1996: Sudden cessation of katabatic winds in Adélie Land, Antarctica. *J. Appl. Meteor.,* **35,** 1129–1141.

Gates, W. L., 1992: AMIP: The Atmospheric Model Intercomparison Project. *Bull. Amer. Meteor. Soc.,* **73,** 1962–1970.

Genthon, C., 1994: Antarctic climate modelling with general circulation models of the atmosphere. *J. Geophys. Res.,* **99** (D6), 12 953–12 961.

——, and A. Braun, 1995: ECMWF analysis and predictions of the surface climate of Greenland and Antarctica. *J. Climate,* **8,** 2324–2332.

Giovinetto, M. B., N. M. Waters, and C. R. Bentley, 1990: Dependence of Antarctic surface mass balance on temperature, elevation, and distance to open ocean. *J. Geophys. Res.,* **95,** 3517–3531.

Hense, A., M. Kerschgens, and E. Raschke, 1982: An economical method for computing radiative transfer in circulation models. *Quart. J. Roy. Meteor. Soc.,* **108,** 231–252.

King, J. C., 1990: Some measurements of turbulence over an Antarctic ice shelf. *Quart. J. Roy. Meteor. Soc.,* **116,** 379–400.

Kodama, Y., and G. Wendler, 1986: Wind and temperature regime along the slope of Adélie Land, Antarctica. *J. Geophys. Res.,* **91** (D6), 6735–6741.

——, ——, and N. Ishikawa, 1989: The diurnal variation of the boundary layer in summer in Adélie Land, eastern Antarctica. *J. Appl. Meteor.,* **28,** 16–24.

Kukla, G., and D. Robinson, 1980: Annual cycle of surface albedo. *Mon. Wea. Rev.,* **108,** 56–58.

Loewe, F., 1970: The transport of snow on ice sheets by the wind. *Studies on Drifting Snow,* U. Radok, Ed., Vol. 13, Meteorological Dept., University of Melbourne, 21–69.

Louis, J. F., 1979: A parametric model of vertical eddy fluxes in the atmosphere. *Bound.-Layer Meteor.,* **17,** 187–202.

Mather, K. B., and G. S. Miller, 1967: Notes on topographic factors affecting the surface wind in Antarctica, with special reference to katabatic winds and bibliography. Geophysical Institute Rep. UAGR-189, University of Alaska, Fairbanks, AK 125 pp.

Mitchell, J. F. B., and C. A. Senior, 1989: The Antarctic winter: Simulations with climatological and reduced sea-ice extents. *Quart. J. Roy. Meteor. Soc.,* **115,** 225–246.

Murphy, B. F., and I. Simmonds, 1993: An analysis of strong wind events simulated in a GCM near Casey in the Antarctic. *Mon. Wea. Rev.,* **121,** 522–534.

Ohmura, A., T. Konzelmann, M. Rotach, J. Forrer, M. Wild, A. Abe-Ouchi, and H. Toritani, 1994: Energy balance for the Greenland ice sheet by observation and model computation. *Snow and Ice Covers; Interactions with the Atmosphere and Ecosystems,* H. G. Jones, T. D. Davies, A. Ohmura, and E. M. Morris, Eds., Vol. 223, IAHS Publishing, 85–94.

——, M. Wild, and L. Bengtsson, 1996: A possible change in mass balance of Greenland and Antarctic ice sheets in the coming century. *J. Climate,* **9,** 2124–2135.

Parish, T. R., and D. H Bromwich, 1987: The surface windfield over the Antarctic ice sheets. *Nature,* **328,** 51–54.

——, and ——, 1991: Continental-scale simulation of the Antarctic katabatic wind regime. *J. Climate,* **4,** 135–146.

Phillpot, H. R., and J. W. Zillman, 1970: The surface temperature inversion over the Antarctic continent. *J. Geophys. Res.,* **75,** 4161–4169.

Robock, A., 1980: The seasonal cycle of snow cover, sea ice and surface albedo. *Mon. Wea. Rev.,* **108,** 267–285.

Roeckner, E., M. Rieland, and E. Keup, 1991: Modelling of cloud and radiation in the ECHAM model. *ECMWF/WCRP Workshop on Clouds, Radiative Transfer and the Hydrological Cycle,* Reading, United Kingdom, ECMWF/WCRP, 199–222.

——, and Coauthors, 1992: Simulation of the present day climate with the ECHAM model: Impact of model physics and resolution. Max-Planck Institute for Meteorology Rep. 93.

Schwerdtfeger, W., 1970: The climate of the Antarctic. *World Survey of Climatology,* S. Orvig, Ed., Vol. XIV, Elsevier, 253–355.

——, 1975: The effect of the Antarctic peninsula on the temperature regime of the Weddell Sea. *Mon. Wea. Rev.,* **103,** 45–51.

——, 1984: Weather and climate of the Antarctic. *Developments in Atmospheric Science,* Vol. 15, Elsevier, 261 pp.

Simmonds, I., 1990: Review: Improvements in General Circulation Model performance in simulating Antarctic climate. *Antarc. Sci.,* **2,** 287–300.

——, and W. F. Budd, 1991: Sensitivity of the Southern Hemisphere circulation to leads in the Antarctic pack ice. *Quart. J. Roy. Meteor. Soc.,* **117,** 1003–1024.

——, and R. Law, 1995: Associations between Antarctic katabatic flow and the upper level winter vortex. *Int. J. Climatol.,* **15,** 403–421.

Smith, S. R., and C. R. Stearns, 1993: Antarctic climate anomalies surrounding the minimum in the Southern Oscillation Index. *Antarctic Meteorology and Climatology, Studies Based on Automatic Weather Stations,* D. H. Bromwich and C. R. Stearns,

Eds., Antarctic Research Series, Vol. 61, Amer. Geophys. Union, 149–174.

Stearns, C. R., L. M. Keller, G. A. Weidner, and M. Sievers, 1993: Monthly mean climatic data for Antarctic automatic weather stations. *Antarctic Meteorology and Climatology, Studies Based on Automatic Weather Stations*, D. H. Bromwich and C. R. Stearns, Eds., Antarctic Research Series, Vol. 61, Amer. Geophys. Union, 1–21.

Stephens, G. L., 1978: Radiation profiles in extended water clouds, 2: Parameterization schemes. *J. Atmos. Sci.*, **35,** 2123–2132.

Sundquist, H., 1978: A parameterization scheme for non-convective condensation including prediction of cloud water content. *Quart. J. Roy. Meteor. Soc.*, **104,** 677–690.

Taljaard, J. J., H. van Loon, H. L. Crutcher, and R. L. Jenne, 1969: Climate of the upper air: Southern Hemisphere. Vol. I, Temperatures, dew points and heights at selected pressure levels. NAVAIR 50-1C-55, Chief Naval Operations, Washington DC, 135 pp.

Tiedtke, M., 1989: A comprehensive mass flux scheme for cumulus parameterization in large-scale models. *Mon. Wea. Rev.*, **117,** 1779–1800.

Tzeng, R.-Y., D. H. Bromwich, and T. R. Parish, 1993: Present-day Antarctic climatology of the NCAR Community Climate Model version 1. *J. Climate*, **6,** 205–226.

——, ——, ——, and B. Chen, 1994: NCAR CCM2 simulation of the modern Antarctic climate. *J. Geophys. Res.*, **99,** 23 131–23 148.

van den Broeke, M. R., 1997: Spatial and temporal variation of sublimation on Antarctica: Results of a high-resolution GCM. *J. Geophys. Res.*, in press.

——, and R. Bintanja, 1995a: On the interaction of katabatic wind and blue ice area formation in East-Antarctica. *J. Glaciol.*, **41,** 395–407.

——, and ——, 1995b: Summer time atmospheric circulation in the vicinity of a blue ice area in east Queen Maud Land, Antarctica. *Bound.-Layer Meteor.*, **72,** 411–438.

van Loon, H., 1967: The half-yearly oscillation in the middle and high southern latitudes and the coreless winter. *J. Atmos. Sci.*, **24,** 472–486.

——, 1972: Pressure in the Southern Hemisphere. *Meteorology of the Southern Hemisphere*, C. W. Newton, Ed., Amer. Meteor. Soc., 59–86.

——, J. J. Taljaard, R. L. Jeune, and H. L. Crutcher, 1971: Climate of the upper air: Southern Hemisphere. Vol. II, Zonal geostrophic winds. NCAR TN/STR-57 and NAVAIR 50-1C-565, 43 pp. [Available from NCAR, P.O. Box 3000, Boulder, CO 80307.]

Walsh, K., and J. L. McGregor, 1996: Simulations of Antarctic climate using a limited area model. *J. Geophys. Res.*, **101** (D14), 19 093–19 108.

Wendler, G., and Y. Kodama, 1984: On the climate of Dome C in relation to its geographical setting. *J. Climatol.*, **4,** 495–508.

——, J. C. André, P. Pettré, J. Gosink, and T. Parish, 1993: Katabatic winds in Adélie coast. *Antarctic Meteorology and Climatology, Studies Based on Automatic Weather Stations*, D. H. Bromwich and C. R. Stearns, Eds., Antarctic Research Series, Vol. 61, Amer. Geophys. Union, 23–46.

Xu, J. S., H. von Storch, and H. van Loon, 1990: The performance of four spectral GCMs in the Southern Hemisphere: The January and July climatology and the semiannual waves. *J. Climate*, **3,** 53–70.

Yasunari, T., and S. Kodama, 1993: Intraseasonal variability of katabatic wind over East Antarctica and planetary flow regime in the Southern Hemisphere. *J. Geophys. Res.*, **98** (D7), 13 063–13 070.